Proceedings of the XVIII ECSMGE 2024
GEOTECHNICAL ENGINEERING CHALLENGES
TO MEET CURRENT AND EMERGING NEEDS OF SOCIETY

ISBN 978-1-032-54816-6
DOI 10.1201/9781003431749-646

ECSMGE 24
XVIII EUROPEAN CONFERENCE ON SOIL MECHANICS AND GEOTECHNICAL ENGINEERING

Thermal characterization of Aveiro soil for multiscale building energy simulation using shallow geothermal system

Caractérisation thermique du sol d'Aveiro pour la simulation énergétique multi-échelle des bâtiments à l'aide d'un système géothermique peu profond

R.B. Roka*
RISCO, Department of Civil Engineering, University of Aveiro, Aveiro, Portugal

A. Vieira
National Laboratory of Civil Engineering, Lisbon, Portugal

A. Figueiredo, C. Cardoso
RISCO, Department of Civil Engineering, University of Aveiro, Aveiro, Portugal

**rajeneraroka@ua.pt*

ABSTRACT: Shallow geothermal energy systems are evolving as an alternative source of energy for building space heating and cooling with notable contributions to carbon emission reduction. In this context, proper soil thermal characterization is crucial for determining the potential of these systems' use and their energy efficiency evaluation. This paper presents the results of the assessment of the physical and thermal characterization of samples retrieved in the city of Aveiro, Portugal. The thermal tests were performed in transient conditions using a needle probe and plane sensor device and the respective results were compared. The study provides some insights regarding Aveiro soil's thermal characteristics which will be further used in building energy simulation of campus buildings integrating shallow geothermal energy systems towards sustainable energy planning and development.

RÉSUMÉ: Les systèmes d'énergie géothermique peu profonde sont en train de devenir une source d'énergie alternative pour le chauffage et la climatisation des bâtiments, avec des contributions notables à la réduction des émissions de carbone. Dans le contexte de la caractérisation thermique des sols, la caractérisation est cruciale pour déterminer le potentiel d'utilisation de ces systèmes et l'évaluation de l'efficacité énergétique. L'article présente l'évaluation de la caractérisation physique et thermique d'échantillons prélevés dans la ville d'Aveiro, au Portugal. Les essais thermiques ont été effectués dans des conditions transitoires à l'aide d'une sonde à aiguille et d'un capteur plan et les résultats respectifs ont été comparés. L'étude fournit quelques informations sur les caractéristiques thermiques du sol d'Aveiro, qui seront ensuite utilisées dans la simulation énergétique des bâtiments du campus intégrant des systèmes d'énergie géothermique peu profonds pour la planification et le développement de l'énergie durable.

Keywords: Shallow geothermal energy; soil thermal conductivity; thermal probes; sustainability.

1 INTRODUCTION

For the space heating and cooling of buildings, low enthalpy ground source systems have been shown as a promising and sustainable source of renewable energy. To harness shallow geothermal energy, it is crucial to assess and determine the thermal parameters of soils as they determine the heat exchange performance between the ground and the buildings to be acclimatized (Del Pozo et al., 2021). Heat transfer processes in soils can occur, through the physical processes: conduction, convection or radiation. However, for these systems, conduction is the dominant process (Vieira et al., 2019). Thermal conductivity quantifies the ability of materials to conduct thermal energy, it is the soil´s most important factor in determining the primary circuit performance of shallow geothermal heat exchangers (Roka et al., 2023). Volumetric heat capacity indicates the amount of heat energy required to raise the temperature of a unit volume of a substance by one degree Celsius or one Kelvin. It's an important parameter when considering the thermal behavior of soil, including its ability to store or release heat (e.g. Kodesová et al., 2013). A proper knowledge of the thermal properties of soil is essential to design the geothermal system as they influence heat extraction from the soil and heat rejection to the soil as well as the performance and efficiency of the geothermal system (Vieira et al., 2017). Several factors influence the soil's thermal

conductivity and heat capacity in particular their index properties such as soil particle distribution, water content, bulk and particle density, degree of saturation, and void ratio (Zeh et al., 2021). Among these, the factors that most influence soil thermal properties are the water content (degree of saturation) and porosity. The mineralogical composition of the soil also has a significant influence on its thermal behavior.

To design an energy simulation model of the campus buildings of Aveiro University with the integration of shallow geothermal systems using whole-building energy simulation software CitySim Pro the knowledge of the heat extraction potential from the soil is crucial. The assessment of information on the thermal properties of Aveiro soils will help to fulfil this purpose.

2 LABORATORY EXPERIMENTS

2.1 Theoretical background: needle and surface probes

The needle sensor is a Transient Line Source (TLS) device for the determination of the thermal conductivity of soil in non-steady state conditions in an infinite medium (e.g. Lockmuller et al., 2003). This technique uses a line heat source, the temperature changes in soil over time are recorded when the heat of a known amount is applied to the sample soil. Carslaw and Jaeger, (1959) give the relation of temperature response at any time t (s) accordingly:

$$T = \frac{q}{4\pi\lambda}\int_x^\infty \frac{e^{-u}}{u}du \quad (1)$$

where q (W.m^{-2}) is the power input per unit area, T (K) is the temperature at any radial distance r(m) from the needle, x is $\frac{r^2}{4\alpha t}$, α (m^2.s^{-1}) is the thermal diffusivity and the thermal conductivity of soil λ (W.m^{-1}.K^{-1}).

In the TLS method, a thin needle heat source is inserted into the soil sample, simulating a linear heat source of infinitesimal radius in a semi-infinite medium. The heat flow within the soil sample follows a radial pattern. The rate of heat propagation in the soil sample is contingent on its thermal conductivity. For soils with high conductivity, the propagation time is notably shorter. Conversely, in soils with lower conductivity, the propagation time is prolonged. This distinction in propagation times provides valuable insights into the thermal characteristics of different soil types, contributing to a more comprehensive understanding of their behavior in response to heat.

When the t (s) is too large, Eq. (1) becomes:

$$T = \frac{q}{4\pi\lambda}\left(ln\frac{4\alpha t}{r^2} - \gamma\right) \quad (2)$$

Where γ represents Euler‘s constant. For a specified medium in a time-space t_1 (s) and t_2 (s) with the heat flux q (W.m^{-2}), equation 3 provides the thermal conductivity. The derived λ (W·m^{-1}·K^{-1}) value should fall within a 5% deviation from the mean value of each test (ASTM, D5334-14).

$$\Delta T = T_2 - T_1 = \frac{q}{4\pi\lambda}.ln\left(\frac{t_2}{t_1}\right) \quad (3)$$

Thermal conductivity is related to thermal diffusivity, material density and specific heat capacity. Equation 2 illustrates the relationship,

$$\lambda = \alpha.\rho.c \quad (4)$$

where ρ (kg.m^{-3}) signifies the soil density, α (m^2.s^{-1}) is thermal diffusivity, and c (J.kg^{-1}.K^{-1}) denotes specific heat capacity.

The international standards ASTM D5334-14 and IEEE 442 provide standard information regarding λ (W.m^{-1}.K^{-1}) measurement techniques for TLS. Thermal conductivity can also be measured by the surface probe or transient plane source (TPS). However, this probe is specially designed for hard soil. The surface probe sensor features elements that function both as a heat source and a temperature sensor. Comprising a robust electrical conducting pattern crafted from thick nickel foil embedded within an insulating Kapton layer, the device exhibits a dual role. The application of consistent heat through electrical power induces changes in the sensor's resistance, denoted as R_t (Ω) which is directly correlated with the corresponding increase in temperature T (K). The time-dependent resistance, R (Ω), is mathematically expressed by equation 5. Comprehensive details regarding the calculations and the specifics of the equation can be referenced in (Gustafsson, 1991).

$$R_t = R_0(1 + \phi.\Delta T_t) \quad (5)$$

where R_0 (Ω) is the initial resistance of the hot disk present in the surface probe, ϕ is the temperature coefficient of resistance (TCR) for the probe and $\Delta T_T=(T_T-T_0)$ is the temperature increase in the sensor concerning the time variable t (s). Also,

$$t = \sqrt{\left(\frac{t_0}{\theta}\right)} \text{ and } \theta = \left(\frac{\alpha^2}{\alpha}\right) \quad (6)$$

where t_o(s) is the time from the start of the transient heating, a signifies a constant that is a measure of the overall size of the resistive pattern (half the side of the hot square or the radius of the hot disk) and θ denotes the characteristic time as in equation 6 (Gustafsson, 1991).

When assuming the sample is infinitely large and has no influence from the boundaries, and the geometry of the disk consists of an n concentric ring with a radius of the outermost ring r (m) and ΔT_T can be expressed with the below equation 7,

$$\Delta T_T = \frac{P_o}{\sqrt[3]{\pi}.r\lambda}.D_T \quad (7)$$

where P_0(W) is the total output power of the probe and D_T is a dimensionless time function and can be written in equation 7 (Gustafsson, 1991).

$$D_T=(n(n+1))^{-2}.\int_0^T \frac{d\sigma}{\sigma 2}.(\sum_{h=1}^{n} h(\sum_{k=1}^{n} k.\ Exp((-h^2+k^2)/4\sigma^2n^2).l_0(h.k/2\sigma^2n^2))) \quad (8)$$

where L_0 is the modified Basel function, h(m) is the thickness of the disk, n is the number of concentric rings in the disk and σ is an integration variable. So, λ (W.m^{-1}.K^{-1}) can be obtained by fitting the experimental data to the straight line given by equation 7, and equation 6 gives thermal diffusivity.

2.2 Sampling and sample preparation

Samples were extracted at a construction site near the University of Aveiro using a tube sampler of 70mm diameter and 140mm length. The samples were extracted from excavation cuts from depths of 1m to 3.5m. After the extraction, they were wrapped with thin plastic to preserve initial moisture and carefully transported to the National Laboratory of Civil Engineering (LNEC) Soil Mechanics laboratory and stored in a temperature and moisture-controlled room. Disturbed samples were also taken from the same place as the intact ones to perform physical characterization tests namely grain size distribution, initial water content, Atterberg limits and particle density. As mentioned, some physical parameters of soil have a paramount effect on the λ (W.m^{-1}.K^{-1}). Figure 1 displays a map indicating the sampling locations. At this stage, three samples were tested. The respective results will be used in the multiscale building energy simulation. The three samples can be seen in Figure 2.

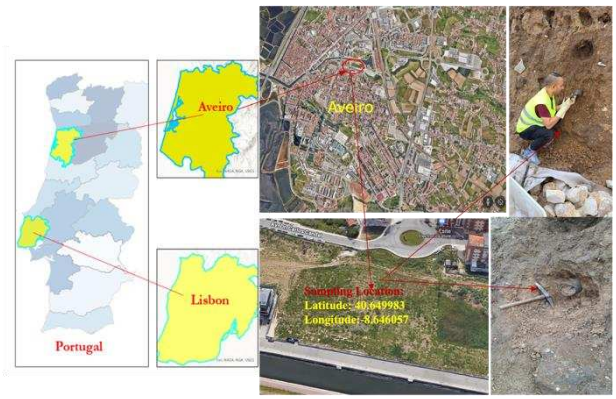

Figure 1. Location map of sampling site in Aveiro.

2.3 Equipment description

For the thermal characterization of samples, equipment comprising a measurement platform, TLS-100vCp and TLS-100 needle sensors and TPS-

Figure 2. Soil samples and their thermal tests.

4 asymmetric (single-sided) sensors were used. Both TLS have a total 100mm needle length. According to ASTM D5334-14, the specimens should be 200±30mm long and 50mm in diameter (ASTM, D5334-14). The user manual of MP-2 mentions that the minimum sample size should be 100mm long and 50mm in diameter. TPS-4 has a sensor diameter of 12.8mm and at least a 35mm diameter sample is recommended for the test recommended by the MP-2 manual (MP-2, 2022). Table 1 presents the spectrum of thermal conductivity measurements and the corresponding accuracy achieved by three distinct sensors, alongside the adhered standards.

2.4 Experimental description

Firstly, the sensor TPS-4 was calibrated by using Pyrex verification sample (λ=1.110W·m^{-1}·K^{-1}) and afterwards both needle sensors with a Polymer verification sample (λ=0.330 W.m^{-1}.K^{-1}) at room temperature 25^{0}C. Additionally, Figure 3 provides a visual representation of the MP-2 device alongside the three sensors.

Table 1. Measurement range of sensors (MP-2, 2022).

Sensor's type	Range of λ ($W \cdot m^{-1} \cdot K^{-1}$)	Accuracy	Standard followed
TPS-4	0.03-5	±5%	ASTM D5334 & IEEE 442-1981
TLS-100	0.1-5	±5%	ASTM D5334-14 & ISO 22007-2
TLS-100vCp	0.02-5	±5%	ASTM D5334-14

Figure 3. MP-2 device with three sensors.

After the calibration, some tests were carried out in a reference soil (Fontainebleau sand). Aljundi et. al., (2019) have previously measured the thermal conductivity of Fontainebleau sand under different densities and saturation degrees. The λ ($W \cdot m^{-1} \cdot K^{-1}$) value obtained at density 1715 $kg.m^{-3}$ at fully dry condition is 0.344 $W \cdot m^{-1} \cdot K^{-1}$ and fully saturated condition is 2.84 $W \cdot m^{-1} \cdot K^{-1}$. A density of 1690$kg.m^{3}$, which was missing in that study, in fully dry and fully saturated conditions was prepared and the obtained values of λ ($W \cdot m^{-1} \cdot K^{-1}$) are presented in Table 2.

Firstly, the samples were tested by using TPS-4 followed by the two-needle sensors. The top surface of the sample was levelled carefully and a weight of one kilogram was placed above the sensor in order to achieve good contact between the plane sensor and the soil sample as shown in Figure 2. Furthermore, while using the needle probes a thermal paste was used to ensure better contact with the surrounding soil. S6062 and S6063 were soft enough to insert the needle probe whereas for S6061 a hole was made with a metallic rod smaller in diameter than the needle. Special care was taken to insert the needles so as not to damage them.

A series of five measurements were performed for each sample with three sensors. The interval between each measurement should be at least 15 to 20 minutes in order to achieve a thermal equilibrium according to the manual of MP-2, though a minimum of 30 minutes was given to provide enough time for better accuracy in the results.

3 RESULTS AND DISCUSSION

Table 3 showcases information about the specific gravity of the soil particles ρ_s, moisture content w (%), void ratio e, degree of saturation S_r (%), liquid limit L_L (%), plastic limit P_L (%), particle size distribution and soil classifications of the tested samples. The particle size distribution of the three Aveiro samples is shown in Figure 4. It can be observed that S6061 has lesser fine particles with major parts of sand and gravel, whereas S6062 and S6063 have a very similar granulometric composition with more than 60% finer particles and were classified as low plasticity clays.

For the thermal tests, the calibration results with the verification sample fell below ±5% of the known value. Table 4 presents a summary of the results of the thermal tests conducted. Each value corresponds to the average of five determinations. For all cases, the repeatability R(%) obtained was excellent (with differences between measurements lower than 5%). Regarding the thermal conductivity measurements in Fontainebleau sand, as expected the value in fully saturated conditions is much higher (about 8 times more) than that in fully dry conditions. When sand is saturated with water, the air in the pore spaces is displaced. Since water has a higher thermal conductivity than air, the replacement of air with water increases the soil thermal conductivity.

In turn, in Figure 5, the values of the thermal conductivity estimated by the three probes for the different samples are shown. Globally it can be observed that the values measured with the surface probe TPS-4 are almost always inferior to the ones obtained with TLS-100 probes.

Additionally, it is noteworthy that the average difference in thermal conductivity measurements between the TLS-100 and TPS-4 sensors remained below 2% for samples 6062 and S6063. However, in the case of sample S6061, this difference exceeded 12%. The significant disparities in results between the plane source TPS-4 and TLS-100 were particularly evident in the sample with more percentage of sand and gravel. This observation may be attributed to the challenge of achieving 100% contact between the sensor and the sand and gravel, potentially allowing air to enter the gap and influencing the measurements.

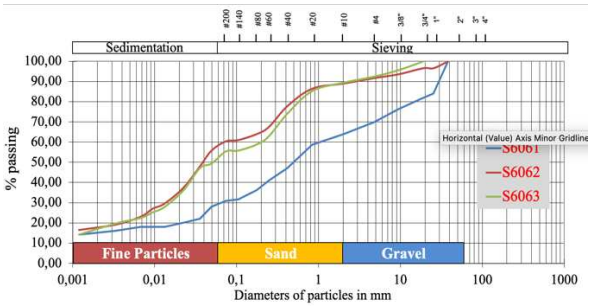

Figure 4. Particle size distribution curves.

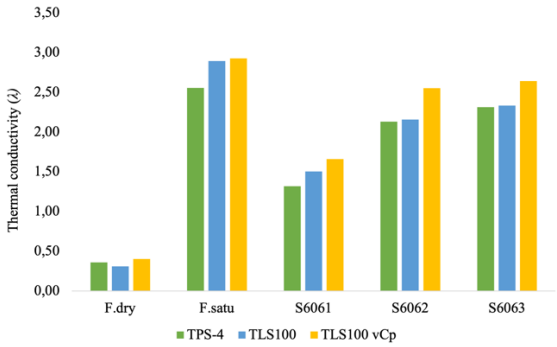

Figure 5. Test results comparison of three sensors.

Regarding measurements conducted with the two needle probes, it is notable that values obtained with probe TLS100-vCp, which incorporates heat capacity measurements, consistently exhibit higher values. On average, the differences relative to the mean are approximately 10%. The thermal conductivity of the samples is influenced by the degree of saturation. Samples S6062 (S_r=91.22%) and S6063 (S_r=92.02%) have higher thermal conductivity values than sample S6061 (S_r=67.22%). However, the relationship is complex and depends on various factors, including mineral composition, and temperature conditions. The measured values of α ($m^2.s^{-1}$) for samples are in the range of $1.0x10^{-6}$ to $3.0x10^{-6}$ $m^2.s^{-1}$. According to Hillel, (1982) the thermal diffusivity of moist soil ranges from $1.0\ x10^{-6}$ to $3.0x10^{-6}$ $m^2.s^{-1}$. Additionally, Abu-Hamdeh, (2003) obtained a volumetric heat capacity value of $1.09\text{-}3.04x10^6$ $J{\cdot}m^{-3}{\cdot}K^{-1}$ and the measured value of C_p ($J{\cdot}m^{-3}{\cdot}K^{-1}$) in this research is $1.053\text{-}2.012x10^6$ $J{\cdot}m^{-3}{\cdot}K^{-1}$ for moist soil.

Table 2 provides information on maximum density ($kg{\cdot}m^{-3}$) and their respective void ratios e^{max}, e^{min}, and e^{cal} for Fontainebleau sand.

Table 2. Maximum, minimum and calculated densities and void ratio of Fontainebleau sand.

Sample	ρ_{max} (kg.m^{-3})	ρ_{min} (kg.m^{-3})	ρ_{cal} (kg.m^{-3})	e^{max}	e^{min}	e^{cal}
Fontainebleau sand	1750	1440	1690	0.855	0.521	0.579

Table 3. Physical properties of the Aveiro samples.

Samples	ρ_s	w (%)	e	Sr (%)	L_L-P_L (%)	Particle size distribution			Soil Classification
						Gravel (%)	Sand (%)	Fines (%)	
Aveiro-S6061	2.66	14.89	0.589	67.22	23.9-19.0	36.2	33.3	30.5	**GC** (Clayey gravel with sand)
Aveiro-S6062	2.67	14.53	0.425	91.22	20.2-12.9	10.6	31.3	58.1	**CL** (Lean clay with sand)
Aveiro-S6063	2.74	15.69	0.467	92.02	19.1-13.8	10.6	38.1	51.3	**CL-ML** (Silty clay with sand)

4 FINAL REMARKS

In this work, laboratory-measured values of the thermal properties of Aveiro soils using different thermal probes were presented. Values of the physical properties of these soils were also provided, along with data recorded on a reference soil. All measurements were conducted under non-steady-state heat flow conditions. Overall, the obtained values are typical values of the tested soil types, and very good repeatability was obtained. It was observed that the thermal conductivity values measured with the surface probe were consistently lower than those measured with the needle probes. This difference may be attributed to heat losses, contact issues, or the analytical approximations underlying this determination.

On the other hand, it is also not clear why there is a difference in measurements between the two needle probes with the probe that also allows obtaining thermal diffusivity values giving consistently higher values. According to the manufacturer, the conductivity values, in this case, are estimated based on an iterative calculation performed during the test based on the line source solution expression, which enables the simultaneous evaluation of λ ($W.m^{-1}.K^{-1}$) and α ($m^2.s^{-1}$) but not on a direct determination of λ ($W.m^{-1}.K^{-1}$). Further investigations, encompassing numerical replication of evaluation of λ ($W.m^{-1}.K^{-1}$)

Table 4. Thermal characteristics of the Aveiro soil samples by MP-2 platform with three sensors.

Samples	Thermal sensors	Thermal properties		
		λ (W.m^{-1}.K^{-1})	α (m^2.s^{-1})	C_p (J.m^{-3}.K^{-1})
Fontainebleau sand$_{dry}$	TLS-100	0.359	0.562 x10^{-6}	0.717 x10^6
	TLS-100vCp	0.402		
	TPS-4	0.310		
Fontainebleau sand$_{saturated}$	TLS-100	2.892	2.012 x10^{-6}	2.206 x10^6
	TLS-100vCp	2.926		
	TPS-4	2.556		
Aveiro - S6061	TLS-100	1.504	1.053 x10^{-6}	1.561x10^6
	TLS-100vCp	1.660		
	TPS-4	1.319		
Aveiro - S6062	TLS-100	2.158	1.423 x10^{-6}	1.792 x10^6
	TLS-100vCp	2.550		
	TPS-4	2.129		
Aveiro - S6063	TLS-100	2.332	1.575 x10^{-6}	1.679 x10^6
	TLS-100vCp	2.641		
	TPS-4	2.313		

and α (m^2.s^{-1})**.** Further investigations, encompassing numerical replication of the test, are underway as part of this study's scope.

ACKNOWLEDGEMENTS

The authors are grateful for the financial support provided by the Foundation of Science and Technology (FCT) to the first author with PhD grant number (2022.10333.BD); equipment and laboratory support from project GeoSustained (PTDC/ECI-CON/1866/2021) and National Laboratory of Civil Engineering (LNEC).

REFERENCES

Abu-Hamdeh, N. H. (2003). Thermal properties of soils as affected by density and water content. *Biosystems Engineering*, *86*(1), 97–102. https://doi.org/10.1016/S1537-5110(03)00112-0.

Aljundi, K., Vieira, A, Maranha, J. R., Lapa, J., & Figueiredo, A. (2019). Some aspects of measurement of sand thermal conductivity from laboratory tests, In: International Society for Soil Mechanics and Geotechnical Engineering, Reykjavik, Iceland. https://doi.org/10.32075/17ECSMGE-2019-0541.

ASTM (D5334-14). ASTM D5334-14, Standard Test Method for Determination of Thermal Conductivity of Soil and Soft Rock by Thermal Needle Probe Procedure, ASTM International, West Conshohocken, USA.

Carslaw and Jaeger. (1959). *Conduction of heat in solids*, Oxford Science Publications, Oxford, UK.

Del Pozo, S., Sáez-Blázquez, C., Martín Nieto, I., & Lagüela, S. (2021). Integrated approach for detecting convection effects in geothermal environments based on TIR camera measurements. *Applied Sciences*, 11(7), https://doi.org/10.3390/app11073185.

Gustafsson, S. E. (1991). Transient plane source techniques for thermal conductivity and thermal diffusivity measurements of solid materials, *Review of Scientific Instruments,* 62(3), (797–8049), https://doi.org/10.1063/1.1142087.

Hillel, D. (1982). *Introduction to Soil Physics* 1st Edition, Academic Press, California, USA.

Kodesová, R., Vlasáková, M., et.al., (2013). Thermal properties of representative soils of the Czech Republic. *Soil and Water Research*, 8(4), 141–150. https://doi.org/10.17221/33/2013-swr.

Lockmuller, N., Redgrove, J., & Kubičár, L. (2003). Measurement of thermal conductivity with the needle probe. *High Temperatures - High Pressures*, 35–36(2), 127–138. https://doi.org/10.1068/htjr099.

MP-2, (2022). Measurement platform-2, *User Manual*, Thermtest portable.

Roka, R. B., de Figueiredo, A. J. P., Vieira, A. M. C. P., & Cardoso, J. C. de P. (2023). A systematic review on shallow geothermal energy system: a light into six major barriers, *Soils and Rocks,* 46(1), https://doi.org/10.28927/SR.2023.007622.

Vieira, A., Alberdi-Pagola, M., Christodoulides, P., Javed, et.al., (2017). Characterisation of Ground Thermal and Thermo-Mechanical Behaviour for Shallow Geothermal Energy Applications, *Energies*, 10(12), (2044), https://doi.org/10.3390/EN10122044.

Vieira, A., Alberdi-Pagola, M., Barla, et.al., (2022). Site characterization for the design of thermoactive geostructures, *Soils and Rocks*, 45(1), https://doi.org/10.28927/SR.2022.001022.

Zeh, R., Ohlsen, B., Philipp, D., Bertermann, D., Kotz, T., Jocić, N., & Stockinger, (2021). Large-scale geothermal collector systems for 5th generation district heating and cooling networks, *Sustainability*, 13(11), https://doi.org/10.3390/su13116035.